



OPEN

Assessment of economic, thermal and hydraulic performances a corrugated helical heat exchanger filled with non-Newtonian nanofluid

Muhammad Ibrahim¹, Ebrahim A. Algehyne², Tareq Saeed³, Abdallah S. Berrouk^{4,5}, Yu-Ming Chu^{6,7}✉ & Goshtasp Cheraghian⁸✉

Improved heat transfer efficiency with considering economic analysis in heating systems is an interesting topic for researchers and scientists in recent years. This research investigates the heat transfer rate (HTR) and flow of non-Newtonian water-Carboxyl methyl cellulose (CMC) based Al_2O_3 nanofluid in a helical heat exchanger equipped with common and novel turbulators using two-phase model. The requirements for dimensions and cost reduction and also energy saving in thermal systems are the main goal of this study. According to gained results usage of corrugated channel in helical heat exchanger has a considerable influence on thermal and hydraulic performance evaluation criteria (THPEC) index of helical heat exchanger and can improve the THPEC index. Thus, $Re = 5000$ is obtained as an optimum value, in which the maximum THPEC value is achieved. As it is found in this paper, in case of using novel heat exchanger instead of the basic smooth system, the thermal properties (by considering Nusselt number) increases about 210%, the hydraulic performance (friction factor) reduces about 28%, performance evaluation criteria index increases about 57% and the material consumption (in case of similar THPEC) decreases about 31%. In another word, with considering economic analysis for the basic and novel system which has same efficiencies, the novel one has lower length and consequently 31% lower material.

List of symbols

Symbols

A	Area of surface (m^2)
c_p	Specific heat (J/kgK)
D_h	Hydraulic diameter (m)
d	Diameter of nanoparticles (nm)
f	Friction factor
h_{bf}	Heat transfer coefficient of base fluid
k	Thermal conductivity (W/mK)
k_{np}	Thermal conductivity of nanoparticle

¹School of Mathematics and Physics, University of Science and Technology Beijing, Beijing 100083, China. ²Department of Mathematics, Faculty of Science, University of Tabuk, P.O. Box 741, Tabuk 71491, Saudi Arabia. ³Nonlinear Analysis and Applied Mathematics (NAAM)-Research Group, Department of Mathematics, Faculty of Science, King Abdulaziz University, P.O. Box 80203, Jeddah 21589, Saudi Arabia. ⁴Mechanical Engineering Department, Khalifa University of Science and Technology, Sas Al Nakhil Campus, PO Box 2533, Abu Dhabi, United Arab Emirates. ⁵Center for Catalysis and Separation, Khalifa University of Science and Technology, PO Box 127788, Abu Dhabi, United Arab Emirates. ⁶Department of Mathematics, Huzhou University, Huzhou 313000, People's Republic of China. ⁷Hunan Provincial Key Laboratory of Mathematical Modeling and Analysis in Engineering, Changsha University of Science and Technology, Changsha 410114, People's Republic of China. ⁸Technische Universität Braunschweig, 38106 Braunschweig, Germany. ✉email: chuyuming@zjhu.edu.cn; g.cheraghian@tu-braunschweig.de

p	Pressure (Pa)
Q	Heat flux (W)
Re	Reynolds number
Re_{np}	Reynolds number of nanoparticle
T	Temperature (K)
u	Velocity
V_m	Velocity

Greek symbols

α	Thermal diffusion
μ	Dynamic viscosity (Ns/m ²)
ρ	Density (kg/m ³)
φ	Nanoparticles volume fraction

Subscriptions

bf	Base fluid
nf	Nanofluid
np	Nanoparticle

Various experimental, analytical and numerical investigations are published due to intensifying the heat transferred amount in heat exchangers. The key aim of these researches is improvement in the heat transfer coefficient (HTC) with the minimum pressure drop. Recent study has been concentrated on the two effective techniques for HTR increment used in the heat exchangers. Vortex generators have been used recently as a typical example of HTR enhancement technique to increase the overall HTC from the fluid or nanofluid flow surface through an upsurge in turbulent motion because of the strong turbulence intensity increase. Nanofluids, which are new type of heat transfer fluids (HTRs), have been used recently also in the heat exchangers as an excellent HTR enhancement technique due to its thermal and physical properties^{1,2}.

Due to the crucial applications of corrugated thermal systems in the apparatus such as heat exchangers, the topic is considered by many researchers^{1–27}. Arie et al.¹ performed an investigation on a manufactured innovative polymer-composite heat exchanger for applications in dry cooling field. Their work pays attention on the thermal characterization and also design of an innovative heat exchanger manufactured by a new process. Their study especially establishes the increasable manufacturing influence in understanding potentially transformative heat exchanger technologies which can also be very problematic for achieving conventional-fabrication methods. Bezaatpour and Rostamzadeh² in a numerical study observed HTR improvement of a fin and tube compact heat exchanger which is under magnetite filed and is filled with ferro-nano-fluid flow. In their study, the influence of a uniform exterior magnetic field on HTR of a heat exchanger filled with Fe₃O₄/water nanofluid was numerically studied. Abeykoon et al.³ designed compact heat exchangers numerically. Numerical and analytical data presented only a 1.05% change in the cooling performance of the hot fluid characteristic. The axial pressure reductions displayed positive correlations with both the pumping power request and the overall HTC. Their achieved results validate that numerical simulation can be talented for optimization, design and manufacturing of thermal systems.

Saleh et al.⁴ carried out a numerical study on wire finned heat exchanger using aluminum fumarate for adsorption heat pumps. They investigated the performance of a wire finned and finned microchannel heat exchangers numerically and experimentally. Their numerical method was confirmed using empirical data and represented an excellent agreement between numerical and experimental results. Hagen et al.⁵ investigated a new method to analysis the Rankine cycle using the generic heat exchanger models. Their findings displayed that employing the innovative analysis resulted in lower net power than using the thermodynamic analyses and this behavior is because of working fluid depending pressure reduction penalty in thermal systems. Larwa and Kupiec⁶ considered a horizontal heat exchanger using an analytical method for the heat transfer process. They realized that variations in ground averaged yearly temperature concerns just the subsurface layers in the initial period of exchanging operation.

Naicker and Rees⁷ studied a large borehole heat exchanger array. The main goal in their study was to introduce a reference data set for analysis of large borehole thermal systems and verification of numerical methods. Warner et al.⁸ studied a novel shallow bore ground heat exchanger. Hu et al.⁹ studied numerically and experimentally investigated a PCM solar air heater and its preheating efficiency. This system was designed to improve indoor air quality and thermal comfort conditions. They employed solar energy as a permanent pre-heated air source and reported their results numerically and experimentally. A numerical investigation on the thermal performance enhancement of ground air heaters using sand-bentonite as backfilling material was done by Agrawal et al.¹⁰. Their study also exposed that the factor of thermal performance deterioration surges with the operation duration. Maximum thermal performance deterioration factor is obtained for ground-air heat exchanger with dry soil at airflow velocity of 5 m/s after 6 h of continuous operation. Minimum thermal performance deterioration factor is observed for ground-air heat exchanger system with wet sand-bentonite. Wen et al.¹¹ observed that the amplitude upsurge and wavelength reduction result in heat transfer area and larger flow length of the corrugated channel, as well as higher HTR. The corrugated channel improves HTR compared to smooth channel. A numerical investigation on airside characteristics of sinusoidal corrugated heat exchangers subject to large-diameter tubes with round or oval cross-section tubes were investigated by Chu et al.¹². The CFD technique has also been adopted to examine complete local heat transfer presentation. Moreover, Yu et al.¹³ used longitudinal

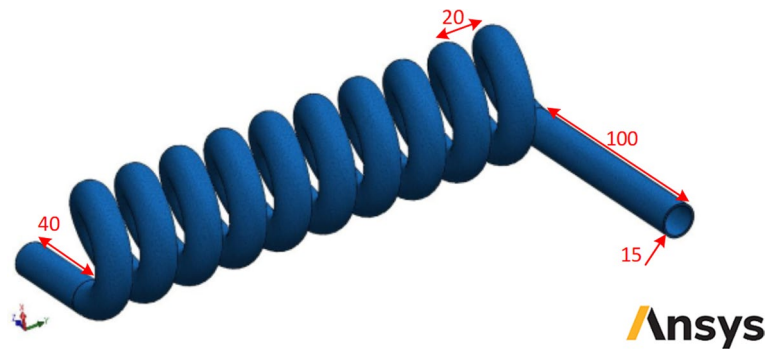


Figure 1. Schematic of studied smooth helical heat exchanger (Images used courtesy of ANSYS, Inc.).

turbulators in a new compound parallel flow shell-and-tube heat exchanger to evaluate turbulent heat transfer. Experimental, analytical, mathematical and numerical investigations showed that the baseline geometry results in the best thermal performance. The increase of the LVG height and LVG attack angle may enhance the THPEC.

Employing horizontal flat-panel ground heat exchangers in ground-coupled heat-pumps was investigated by Habibi et al.¹⁴ numerically. Their achieved data present that even though growing buried depth leads to intensification in the thermal characteristic, the improvement rate reduces sharply when the ground heat exchanger is more than ten meter wide. Kerme and Fung¹⁵ studied in a numerical study heat transfer simulation, examination and presentation study of a single U-tube borehole heat exchanger. Their obtained results may significantly decrease the devoted time for investigation and to more rapid determination the impact of different parameters on vertical single U-tube borehole heat exchanger performance. Additionally, their achieved data can be used as a reference for cooling and heating system optimization and design integrated with system of ground coupled heat pump.

Keshavarz Moraveji et al.²⁸ examined the heat transfer distribution of non-Newtonian nanofluids (NNNFs) in a horizontal-smooth tube under the steady state heat flux, numerically. The studied NNNF included an aqueous solution based Al_2O_3 with various nanoparticles sizes. Their achieved data indicates that the nanofluid HTC and predicted mean Nusselt numbers upsurge in the most non-Newtonian base fluid viscosity values. Akbari et al.²⁹ studies numerically fluid flow and heat transfer distribution of a NNNF through a two-dimensional channel with rectangular cross-section. Their achieved data demonstrated that solid particles adding with various diameters to the base fluid upsurses the HTR in studied microchannel. Minea³⁰ analyzed the turbulent flow and heat transfer distribution of water based Al_2O_3 nanofluid with various volume fractions of nanoparticles in a tube with micro-size. Their results showed that the enhancement of nanofluid HTC is remarkable and has been raised significantly by increasing the nanoparticles volume fraction. Zeinali Heris et al.³¹ studied during a numerical investigation fluid flow and heat transfer distribution of nanofluid flow in a circular pipe. They found that the solid particles may lead to an enhancement in the HTR. In recent years, interesting and diverse studies have been conducted in these fields^{32–41}.

It should be noted that in most aforementioned investigation, the impact of different ribs and corrugations on hydraulic and thermal behavior of base fluid or nanofluids flowing in ducts has been investigated employing single phase model^{42,43}. However, the literature review shows that the effect of novel turbulators (with minimum pressure drop error) on the hydraulic and thermal performance of two-phase NNNF has rarely been described.

Thus, the novelties of this article are as follows:

- Description of the thermal and hydraulic behavior of nanofluids flowing in a heat exchanger with novel turbulators using ANSYS FLUENT 18⁴⁴ software.
- Evaluation of the impacts of using dissimilar types of turbulators on thermal–hydraulic characteristics.
- Investigating the impacts of different values of ϕ and various nanoparticle diameters on thermal and hydraulic behavior.
- In the simulation, two-phase modelling for nanofluid is used.

Numerical model

Physical model. The schematic of studied smooth helical heat exchanger has been presented in Fig. 1. Moreover, Figs. 2 and 3 show the schematic diagram of studied helical heat exchanger equipped with corrugations. In addition, the geometrical properties and configuration of turbulators are presented in this figure. The dimensional properties of the studied heat exchanger have been reported in Figs. 1, 2 and 3. The geometrical dimensions of the heat exchanger are the same for all considered configurations. In other words, the length and diameter of helical channel are similar for all studied models. Due to simplify the simulation procedure bellow assumptions have been considered³⁹:

- The temperatures of walls are maintained at 400 K.
- There is no leakage between the different connections.
- The heat flux of the shell is ignored.
- The nanofluid properties are a function of temperature, volume fraction and particle sizes.

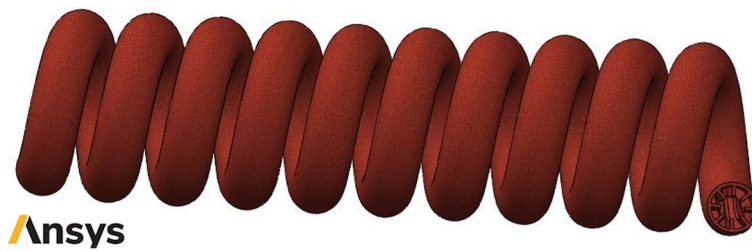


Figure 2. Schematic of studied helical heat exchanger with common turbulators (Images used courtesy of ANSYS, Inc.).

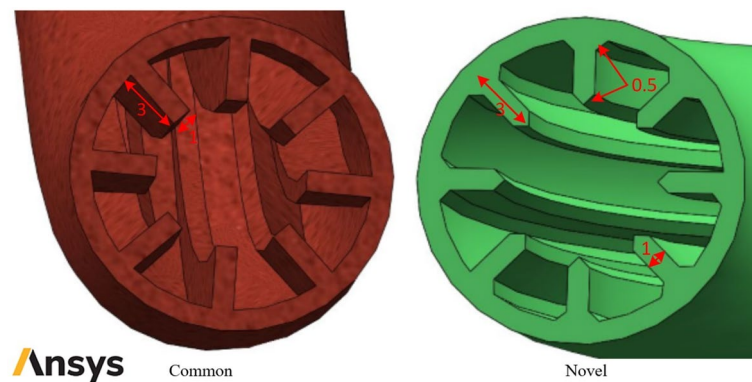


Figure 3. Schematic diagram of studied helical heat exchanger with different turbulators (Images used courtesy of ANSYS, Inc.).

- Differences in hydric diameter are negligible.

Conservation equations. The conservation equations system (energy, momentum, continuity) for two-phase NNNF in the helical heat exchanger may be inscribed as^{39–41}:

$$\nabla \cdot (\rho_{nf} V_m) = 0 \quad (1)$$

ρ_{nf} is the nanofluid density and V_m is the average velocity in each section.

$$\nabla \cdot (\rho_{nf} V_m V_m) = -\nabla P + \nabla \cdot (\mu_{nf} \nabla V_m) \quad (2)$$

μ_{nf} is the viscosity of nanofluid.

$$\nabla \cdot (\rho_{nf} c V_m T) = \nabla \cdot (k_{nf} \nabla T) \quad (3)$$

The supposition of dynamic viscosity behavior for the two-phase NNNF flow in solution field is observed by using of the non-Newtonian two-phase power-law method. The two-phase non-Newtonian power-law viscosity technique can be written as⁴²:

$$\tau = K \dot{\gamma}^n \quad (4)$$

For viscosity and conductivity used equations in⁴⁵.

The Reynolds stress is molded using standard k - ε turbulence model.

$$(-\rho \overline{u_i' u_j'}) = \mu_t \left(\frac{\partial u_i}{\partial x_j} + \frac{\partial u_j}{\partial x_i} \right) \quad (5)$$

$$\mu_t = \rho C_\mu \left(\frac{k^2}{\varepsilon} \right) \quad (6)$$

$$\frac{\partial}{\partial x_i} [\rho k u_i] = \frac{\partial}{\partial x_j} \left[\left(\mu + \frac{\mu_t}{\sigma_k} \right) \frac{\partial k}{\partial x_j} \right] + G_k - \rho \varepsilon \quad (7)$$

$$\frac{\partial}{\partial x_i} [\rho \varepsilon u_i] = \frac{\partial}{\partial x_j} \left[\left(\mu + \frac{\mu_t}{\sigma_\varepsilon} \right) \frac{\partial \varepsilon}{\partial x_j} \right] + C_{1\varepsilon} \frac{\varepsilon}{k} G_k + C_{2\varepsilon} \rho \frac{\varepsilon^2}{k} \quad (8)$$

G_k is the turbulent kinetic energy generation rate and $\rho\varepsilon$ is the dissipation rate and defined by:

$$G_k = \left(-\rho \overline{u'_i u'_j} \right) \left(\frac{\partial u_j}{\partial x_i} \right) \quad (9)$$

The coefficients $Pr_t = 0.9$, $\sigma_\varepsilon = 1.3$, $\sigma_k = 1.0$, $C_{1\varepsilon} = 1.44$, $C_{2\varepsilon} = 1.92$ and $C_\mu = 0.09$ are selected as experimental coefficients in turbulence transport equation³⁹.

Due to analyze the two-phase NNNF flow characteristics and HTR of several turbulators shapes in the helical heat exchanger, definite descriptions have been assumed as^{41–49}:

The Reynolds number (Re) has been expressed as:

$$Re = \frac{\rho_{nf} V_m D_h}{\mu_{nf}} \quad (10)$$

where V_m is fluid mean velocity.

The mean predicted Nusselt number (Nu_{av}):

$$Nu_{av} = \frac{h D_h}{k_{nf}} \quad (11)$$

where h_f and k_f are respectively the mean predicted HTC and thermal conductivity of non-Newtonian base fluid.

The pressure drop between the inlet and outlet is:

$$\Delta p = p_{avg,inlet} - p_{avg,outlet} \quad (12)$$

The average friction factor is³³:

$$f = \frac{2}{\left(\frac{L}{D_h} \right)} \left(\frac{\Delta p}{\rho_{nf} V_m^2} \right) \quad (13)$$

The Thermal and hydraulic performance evaluation criteria (THPEC) is employed to calculate the performance of turbulators to improve HTR assuming the accretion of pumping power. Hence, Nu_{av} and mean friction factor are considered as follows^{41–49}:

$$THPEC = \left(\frac{Nu_{av}}{Nu_{av,s}} \right) \left(\frac{f}{f_s} \right)^{-\frac{1}{3}} \quad (14)$$

where Nu_{av} and $Nu_{av,s}$ are the predicted mean Nusselt number for helical channel equipped with turbulators or filled with two-phase NNNF and the smooth channel or channel filled with non-Newtonian base fluid. Also, f and f_s are the friction factor for channel equipped with turbulators or filled with two-phase NNNF and the smooth channel or channel filled with non-Newtonian base fluid, respectively.

HTR in helical heat exchanger occupied with NNNF for two-phase flow is obtainable as follow³⁹:

$$\dot{Q} = \dot{m} C_{ps} (T_{s,in} - T_{s,out}) \quad (15)$$

The commercial finite volume-based CFD code ANSYS FLUENT (version 18.1) has been employed in current investigation to perform the simulations. For the numerical approach, the velocity–pressure coupled equations are employed. Due to achieve a noteworthy accuracy, SIMPLEC algorithm is implemented. The maximum 10^{-8} error is considered for all parameters to economize the numerical procedure. The *Eulerian–Eulerian* single-fluid *Two-Phase Model* (TPM) are used to solve the governing equations. It should be noted that the phases linking is resilient, and particle prudently shadow the non-Newtonian two-phase nanofluid flow^{46–56}.

The Eulerian–Eulerian two-phase method is based on the assumption that the base fluid particles and nanoparticles move at different speeds but have the same temperature. In fact, in this method, two momentum equations and one energy equation are solved.

For fluid boundary layer influences simulating near walls, solution the Navier–Stokes relations employing evaluate skin friction and the k – ε turbulence model in fluid fields a wall function approach has been employed in Launder and Spalding⁵⁷ approach. However, the ANSYS FLUENTs Flow Simulation (SWFS), instead of using logarithmic profile, employs Van-Driest's profiles. Besides, a *Two-Scale Wall Functions* (2SWF) technique has been implemented to express a turbulent and fluid boundary layers profile compared to Driest⁵⁸ model. More than ten the laminar boundary layers simulation has been completed employing Navier–Stokes equations for cells quantities. Driest⁵⁸ and Van Driest mixing length employs following dependency of the dimensionless longitudinal velocity u^+ on the dimensionless wall distance y^+ to precede turbulent boundary layers from the ANSYS FLUENTs Flow Simulations.

Material	ρ (kg/m ³)	c_p (kJ/kg·K)	k (W/m·K)	μ_0 (Pa.s)
Pure Water	997.1	4.179	613×10^{-3}	1×10^{-3}
CMC	700	0.715	0.15×10^{-3}	1.5
Al ₂ O ₃	3970	0.765	40	—

Table 1. The thermophysical properties of the non-Newtonian base fluid and nanoparticles^{59,60}.

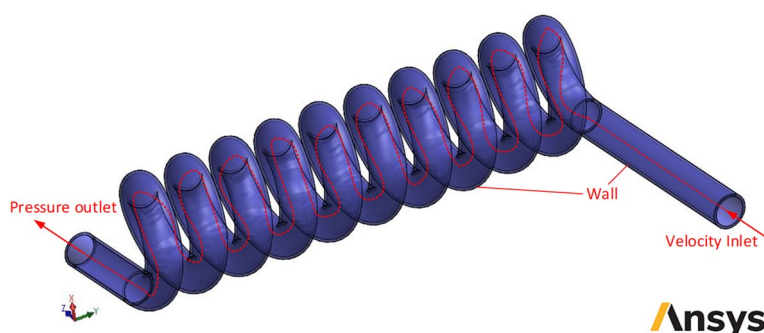


Figure 4. Schematic diagram of boundary conditions in studied helical heat exchanger (Images used courtesy of ANSYS, Inc.).

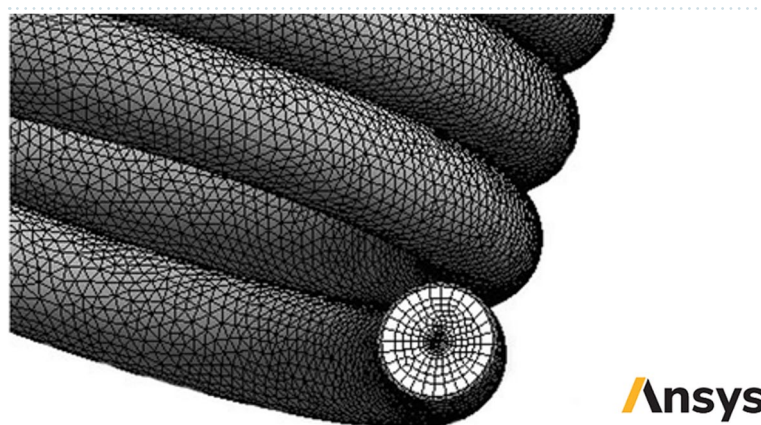


Figure 5. The images of unstructured tetrahedral grids in present study (Images used courtesy of ANSYS, Inc.).

$$u^+ = \frac{u}{\sqrt{\frac{\tau_w}{\rho}}} \int_0^{y^+} \frac{2d\eta}{1 + \sqrt{1 + 4K^2\eta^2 \left(1 - e^{-\frac{\eta}{A_v}}\right)^2}} \quad (16)$$

where A_v is the Van Driest coefficient and is equal to 26. Moreover, K is the Karman constant and is equal to 0.4504. The diffusive heat flux and be determined by the following equation⁵¹:

$$q_i = \left(\frac{\mu}{Pr} + \frac{\mu_t}{\sigma_c} \right) \frac{\partial h}{\partial x_i} \quad i = 1, 2, 3 \quad (17)$$

in which, h refers to the thermal enthalpy, σ_c is the Stephan-Boltzmann constant and is equal to 0.9. Moreover, Pr indicates the Prandtl number. It must be mentioned that available equations express both regimes of laminar and turbulent flows. For purely laminar flow, μ_t and k are zero. The employed boundary conditions for two-phase non-Newtonian nanofluid HTR and flow distribution simulation are expressed as:

1. Total solid domains are known as non-slip conditions.
2. The shell wall is assumed adiabatic.
3. The velocity inlet boundary condition has been set for the inlet section of the channel.
4. Pressure outlet boundary condition is applied to the channel outlet.

No	Nodes	Nu
1	482,154	83.58
2	812,010	70.92
3	1,565,841	67.44
4	2,245,615	58.82
5	2,945,462	56.61
6	3,132,341	56.39
7	3,571,657	56.28

Table 2. Grid independence test for sheet and tube collector.

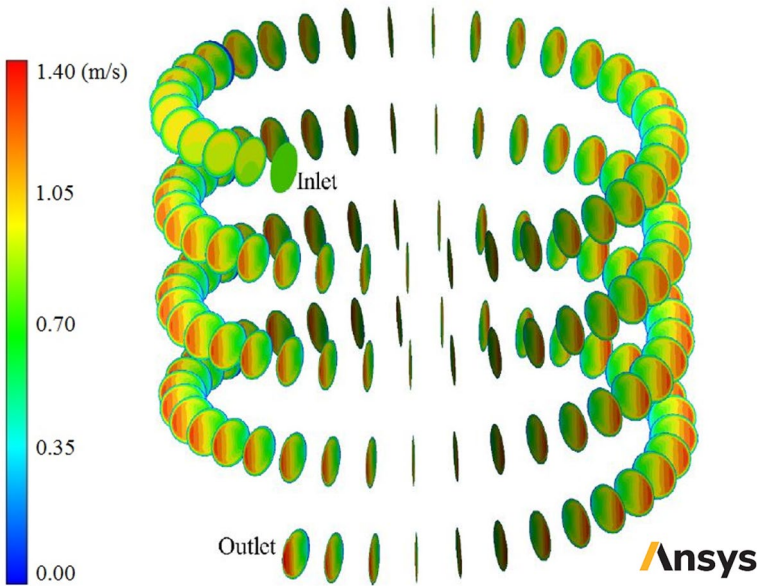


Figure 6. Velocity contours in some cross-sections of smooth-wall helical heat exchanger filled with two-phase NNNF ($\varphi = 1\%$ and $d_{np} = 20\text{ nm}$) (Images used courtesy of ANSYS, Inc.).

	Dittus-Boelter	Mohammed et al. ³⁹	Present study
Re = 2400	21	18	19.6
Re = 3600	30	25.5	27.4
Re = 5600	42	40.5	39.7
Re = 9000	62	57.6	59

Table 3. Comparison between the present results and those of previous works³⁹ and Dittus-Boelter equation.

The inlet fluid temperature for the helical heat exchanger kept constant at 300 K, while the outlet pressure of nanofluid is kept at 100 kPa. The non-Newtonian HTR is H₂O 99.5%:0.5% CMC. To achieve the most efficient NNNF in the current study, Al₂O₃ nanoparticles are added to the non-Newtonian base fluid in different volume concentrations of 1 to 4% with diameters of 20, 30, 40 and 50 nm (Table 1). Also, Fig. 4 shows schematic diagram of boundary conditions in studied helical heat exchanger.

Model validation. The unstructured tetrahedral grid has been designated for the domain because of the complex space of two-phase flow NNNF near walls (see Fig. 5). Table 2 presents the results of the grid study for the conventional collector with water as working fluid using six grid resolutions. The Table demonstrates that the grid resolution of 3,132,341 can provide an excellent agreement between the numerical process cost and the accuracy.

The CFD code verification was done by comparing previous numerical and experimental data and the current study. Figure 6 compares the current findings and the experimental results of Kim et al.⁶¹ and numerical ones of Karimi et al.⁴⁰.

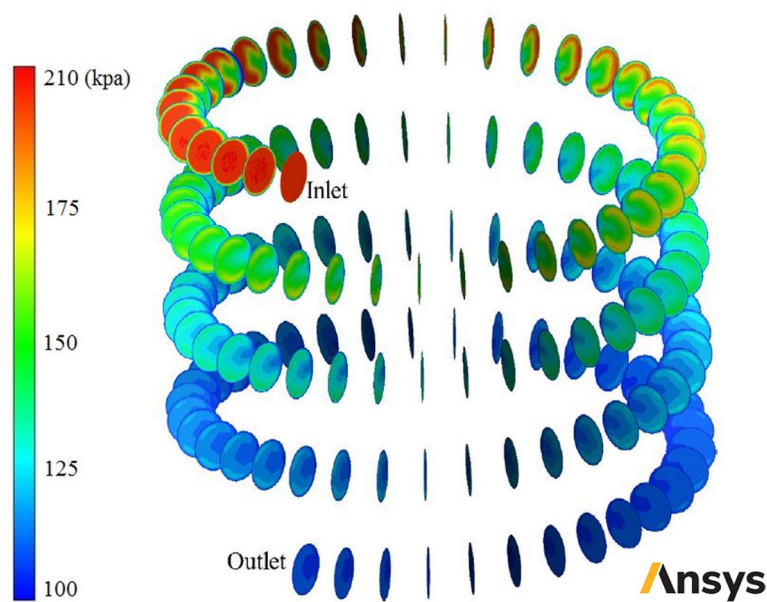


Figure 7. Pressure contours in some cross-sections of smooth-wall helical heat exchanger filled with two-phase NNNF ($\phi = 1\%$ and $d_{np} = 20$ nm) (Images used courtesy of ANSYS, Inc.).

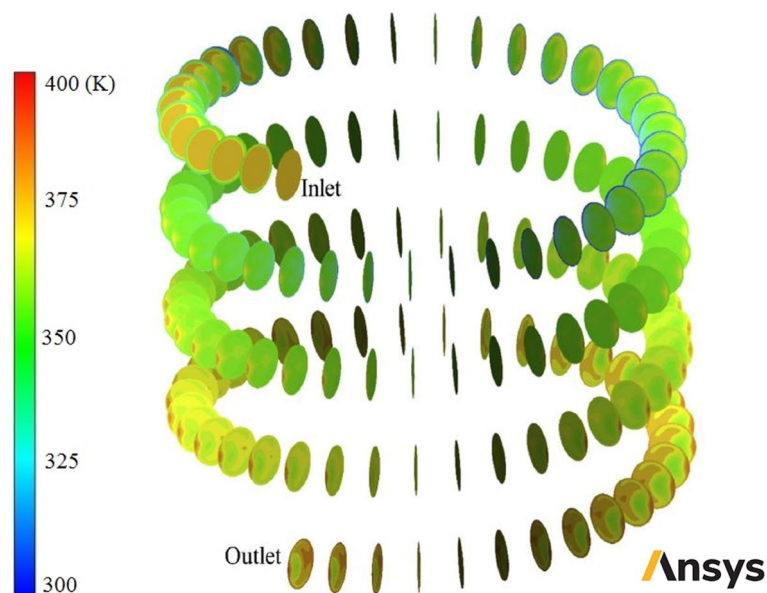


Figure 8. Temperature contours in some cross-sections of smooth-wall helical heat exchanger filled with two-phase NNNF ($\phi = 1\%$ and $d_{np} = 20$ nm) (Images used courtesy of ANSYS, Inc.).

Table 3 also compares the present results with those of previous works³⁹ and Dittus-Boelter equation ($Nu = 0.023Re^{0.8}Pr^{0.4}$) for a tube saturated with pure water and nanofluid, indicating excellent agreement between the previous results and the present ones.

Results and discussion

In this section, usage of corrugated wall helical heat exchanger with different turbulators shapes is investigated and in then usage of nanofluid as heat transfer fluid with different ϕ and diameters is analyzed. In the first stage some contours are reported and the fluid flow and heat transfer field are analyzed. Figure 6 shows velocity contours in some cross-sections of smooth-wall helical heat exchanger filled with two-phase NNNF ($\phi = 1\%$ and $d_{np} = 20$ nm). Figure 7 demonstrates pressure contours in some cross-sections of smooth-wall helical heat exchanger filled with two-phase NNNF ($\phi = 1\%$ and $d_{np} = 20$ nm). Figure 8 illustrates temperature contours in some cross-sections of smooth-wall helical heat exchanger filled with two-phase NNNF ($\phi = 1\%$ and $d_{np} = 20$ nm).

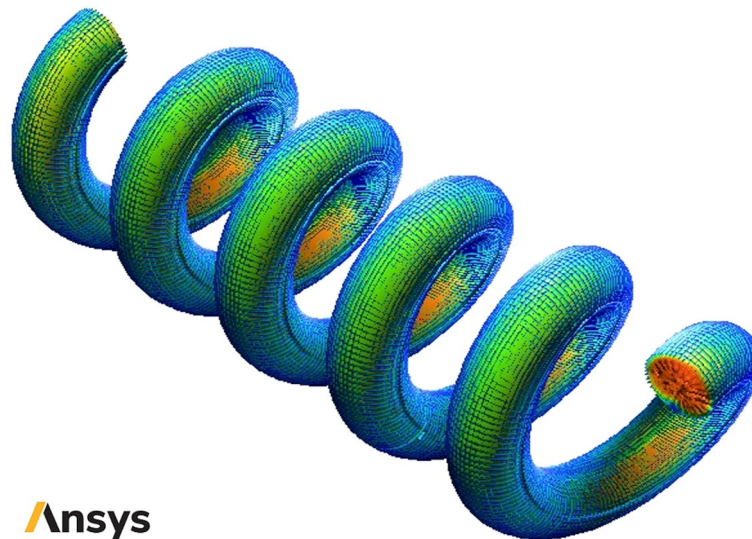


Figure 9. Velocity contour in smooth-wall helical heat exchanger filled with two-phase NNNF ($\phi = 1\%$ and $d_{np} = 20$ nm) (Images used courtesy of ANSYS, Inc.).

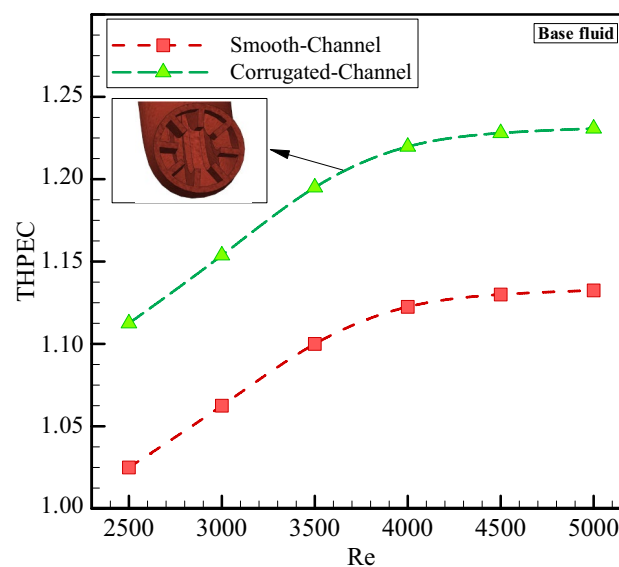


Figure 10. Geometrical effects on THPEC variation versus Re in helical heat exchanger filled with base fluid.

Figure 9 represents velocity contour in smooth-wall helical heat exchanger filled with two-phase NNNF ($\phi = 1\%$ and $d_{np} = 20$ nm).

Optimum geometry. Figure 10 represents geometrical effects on THPEC index variation versus Re in helical heat exchanger filled with base fluid. This figure shows that using corrugated channel in helical heat exchanger has a significant influence on THPEC index of heat exchanger and can improve the THPEC index in heat exchanger about 10%. Also, it is found that the THPEC index value always increases by increase of Re. Therefore, there is an optimum Re, in that the maximum THPEC value is achieved in is Re = 5000. It is clear that in case of using turbulators two parameters have increase: Nu_{av} and pressure reduction penalty. The vortices and turbulent sub-layers increase the HTC in channel and also lead to more pressure drop in channel. But the THPEC index analyze the both above parameters with each other and when the THPEC is more than 1, usage of turbulators is in view point of thermal and hydraulic performance appropriate and efficient. The THPEC index can also help us to analyze the performance of using nanofluid in heat exchangers. If the THPEC will more than 1, employing nanofluid is in view point of thermal and hydraulic performance appropriate and efficient. Therefore, in the next step usage of nanofluid in heat exchanger is investigated. Figure 11 illustrates the THPEC

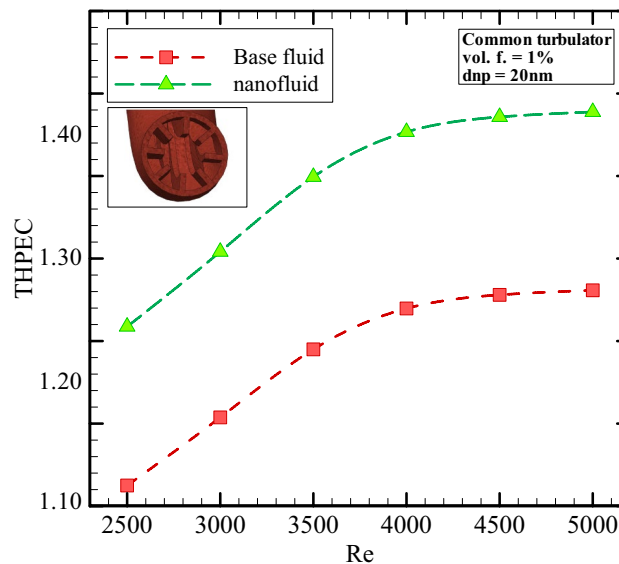


Figure 11. The THPEC index variation versus Re in helical heat exchanger filled with base fluid and nanofluid ($\phi = 1\%$ and $d_{np} = 20\text{ nm}$).

variation versus Re in helical heat exchanger saturated with base fluid and nanofluid ($\phi = 1\%$ and $d_{np} = 20\text{ nm}$) and equipped with common turbulators. This figure shows that using nanofluid ($\phi = 1\%$ and $d_{np} = 20\text{ nm}$) in helical heat exchanger equipped with common turbulators has a considerable influence on the THPEC of heat exchanger and can improve the THPEC index in heat exchanger about 11%. Also, it is found that the PEC index value always increases by increase of Re. Therefore, there is an optimum Re, in that the maximum THPEC value is achieved in is Re = 5000. It is clear that in case of employing nanofluid two parameters have increase: Nu_{av} and pressure reduction penalty. The more conductive HTC of nanofluid increase the HTC in channel and the more dynamic viscosity of nanofluid lead to more pressure drop in channel. But the THPEC index analyze the both above parameters with each other and when the THPEC is more than 1, usage of nanofluid is in view point of thermal and hydraulic performance appropriate and efficient.

Figure 9 demonstrates the THPEC variation versus Re in three different helical heat exchangers filled with nanofluid ($\phi = 1\%$ and $d_{np} = 20\text{ nm}$). This figure shows that using turbulators in helical heat exchanger has a considerable influence on the THPEC of heat exchanger.

It is clear that in case of employing turbulators two parameters have increase: heat transfer rate (Nu_{av}) and pressure reduction penalty. The vortexes and turbulent sub-layers increase the HTC in channel and also lead to more pressure drop in channel. But the THPEC index analyze the both above parameters with each other and when the PEC is more than 1, usage of turbulators is in view point of thermal and hydraulic performance appropriate and efficient. Hence it should be noted that in case of using novel turbulators, the value of pressure drop penalty is less than in case of using common turbulators. Therefore, employing novel turbulators leads to more THPEC value than the other corrugated model. It is realized that in case of using novel configuration of turbulators, the THPEC values during all Re are more than other models, which is followed with common turbulators configuration and smooth channel. Also, it is found that the THPEC index value always increases by increase of Re. Therefore, there is an optimum Re, in that the maximum THPEC value is achieved in is Re = 5000.

Optimum nanofluid. In this section different characteristics of nanofluid flow (nanoparticles volume fractions and diameters) are analyzed according to THPEC index.

Figure 10 shows the THPEC variation versus Re in smooth channel helical heat exchanger filled with nanofluid ($d_{np} = 20\text{ nm}$) in different ϕ . This figure shows that using nanofluid in higher volume fractions in heat exchanger with smooth channel leads to more THPEC of heat exchanger and can improve the THPEC index in heat exchanger about 8%.

In addition, it is found that the THPEC index value always increases by increase of Re. Thus, Re = 5000 is an optimum Reynolds number, in which the maximum PEC value is achieved. Employing nanofluid in higher volume fractions two parameters have increase: Nu_{av} and pressure reduction penalty. The more conductive HTC of nanofluid in higher volume concentrations increase the HTC in channel and the more dynamic viscosity of nanofluid in higher volume fractions lead to higher pressure drop in channel. But the THPEC index analyze the both above parameters with each other and when the THPEC is more than 1, usage of nanofluid is in view point of thermal and hydraulic performance appropriate and efficient. For the nanofluid with diameter size of 20 nm and volume fraction of 4% the maximum values of THPEC are achieved for all investigated Re, which is followed with cases $\phi = 3\%$, 2% and 1%, respectively.

Figure 11 shows the THPEC variation versus Re in helical heat exchanger with common turbulators saturated with nanofluid ($d_{np} = 20\text{ nm}$) in different volume fractions. This figure shows that using nanofluid in higher

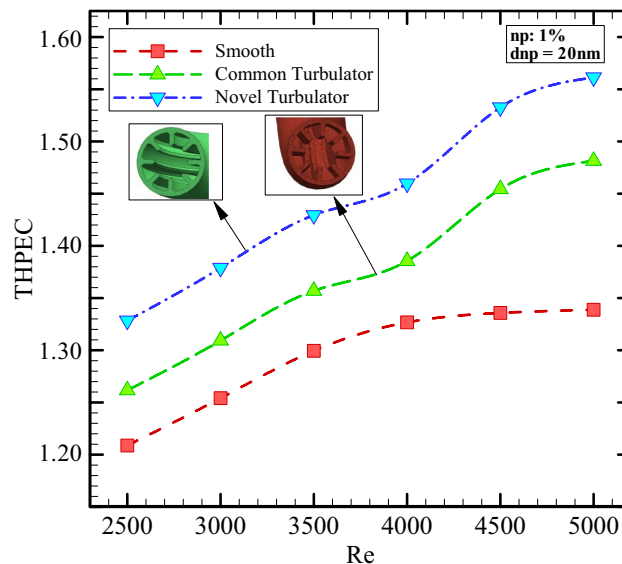


Figure 12. The THPEC index variation versus Re in three different helical heat exchangers filled with nanofluid ($\phi = 1\%$ and $d_{np} = 20\text{ nm}$).

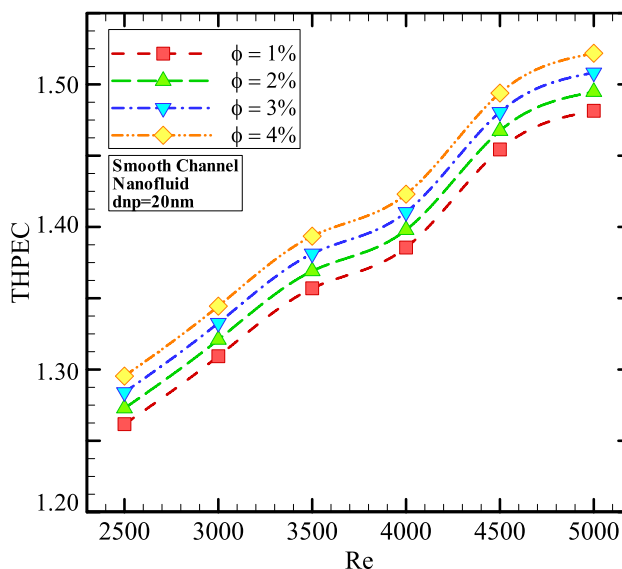


Figure 13. The THPEC variation versus Re in smooth channel helical heat exchanger saturated with nanofluid ($d_{np} = 20\text{ nm}$) in different volume fractions.

volume fractions in heat exchanger equipped with common turbulators results in higher THPEC index of heat exchanger and can improve the THPEC index in heat exchanger about 12%. Also, it is found that the THPEC index value always increases with Re. Thus, $Re = 5000$ is an optimum Reynolds number, in which the maximum THPEC value is achieved. Employing nanofluid in higher volume fractions two parameters have increase: Nu_{avg} and pressure reduction penalty. More conductive HTC of nanofluid in higher volume concentrations increase the HTC in channel and the more dynamic viscosity of nanofluid in higher volume fractions lead to more pressure drop in channel. But the THPEC index analyze the both above parameters with each other and when the THPEC is more than 1, usage of nanofluid is in view point of thermal and hydraulic performance appropriate and efficient. For the nanoparticles with diameter size of 20 nm and volume fraction of 4% the maximum values of THPEC are achieved for all investigated Re, which is followed with cases $\phi = 3\%$, 2% and 1%, respectively.

Figure 12 shows the THPEC variation versus Re in helical heat exchanger with novel turbulators saturated with nanofluid ($d_{np} = 20\text{ nm}$) in different volume fractions. This figure shows that using nanofluid in higher volume fractions in helical heat exchanger equipped with novel turbulators results in higher THPEC index of heat exchanger and can improve the THPEC index in heat exchanger about 13%. Also, it is found that the THPEC

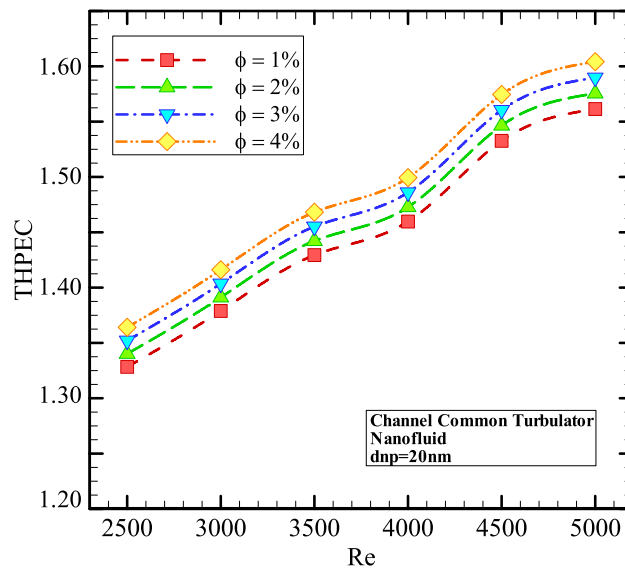


Figure 14. The THPEC variation versus Re in helical heat exchanger equipped with common turbulators saturated with nanofluid ($d_{np} = 20$ nm) in different volume fractions.

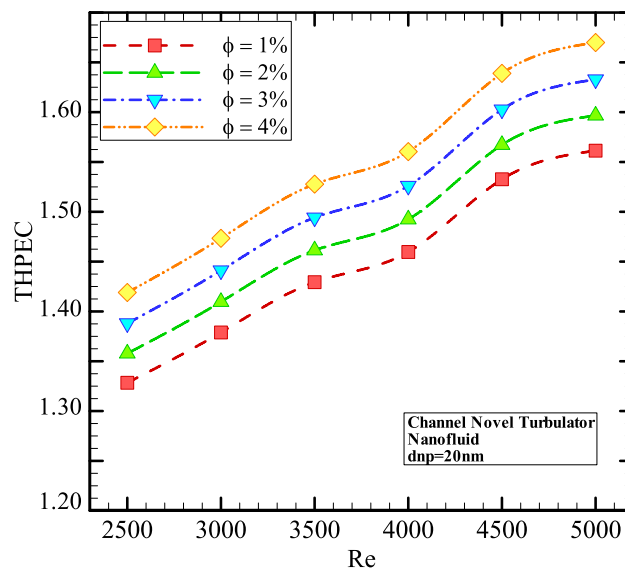


Figure 15. The THPEC variation versus Re in helical heat exchanger with novel turbulators saturated with nanofluid ($d_{np} = 20$ nm) in different volume fractions.

index value always increases by increase of Re. Thus, $Re = 5000$ is an optimum Reynolds number, in which the maximum THPEC value is achieved. Employing nanofluid in higher volume fractions two parameters have increase: Nu_{avg} and pressure reduction. The more conductive HTC of nanofluid in higher volume concentrations increase the HTC in channel and the more dynamic viscosity of nanofluid in higher volume fractions lead to higher pressure drop in channel. But the THPEC index analyze the both above parameters with each other and when the THPEC is more than 1, usage of nanofluid is in view point of thermal and hydraulic performance appropriate and efficient. For the nanofluid with diameter size of 20 nm and volume fraction of 4% the maximum values of THPEC are achieved during all investigated Re, which is followed with cases $\phi = 3\%$, 2% and 1%, respectively.

Figures 13, 14, 15 and 16 show the THPEC variation versus Re in helical heat exchanger with novel turbulators saturated with nanofluid ($\phi = 4\%$) in different nanoparticles diameters. This figure reveals that using nanofluid in higher nanoparticles diameters in heat exchanger with novel turbulators leads to higher THPEC index of heat exchanger and can improve the THPEC index in heat exchanger about 15%. Also it is found that the THPEC index value always increases by increase of Re. Thus, $Re = 5000$ is an optimum Reynolds number, in which the maximum THPEC value is achieved. Employing nanofluid in higher nanoparticles diameters two

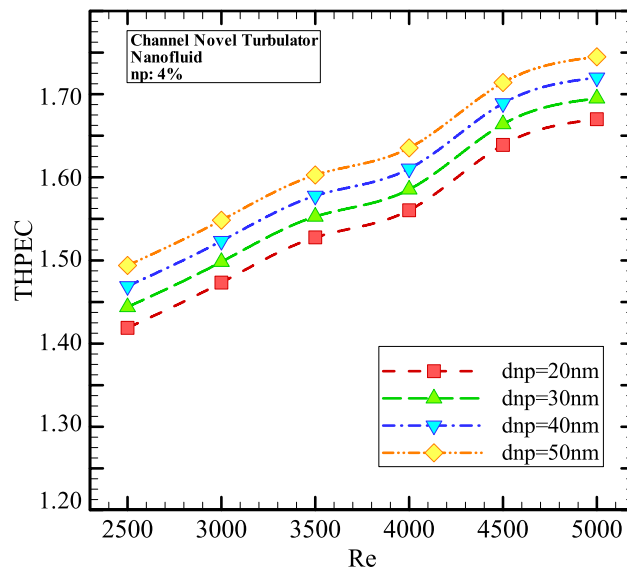


Figure 16. The THPEC variation versus Re in helical heat exchanger with novel turbulators saturated with nanofluid ($\phi = 4\%$) in different nanoparticles diameters.

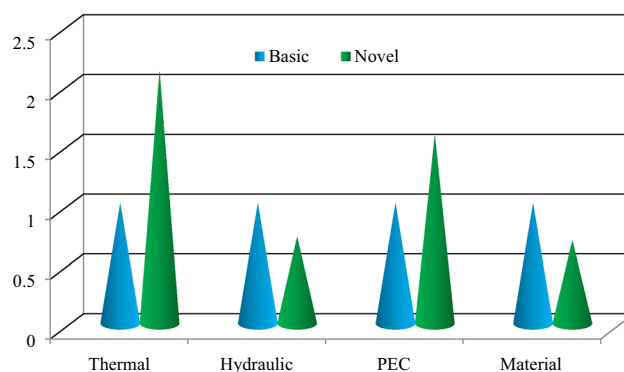


Figure 17. Economic and THPEC variation at Re = 5000 in helical heat exchanger with novel turbulators saturated with nanofluid ($\phi = 4\%$ and $d_{np} = 50$ nm) in comparison with basic system.

parameters have increase: Nu_{avg} and pressure reduction penalty. The more conductive HTC of nanofluid in higher nanoparticles diameters increase the HTC in channel and the more dynamic viscosity of nanofluid in higher nanoparticles sizes lead to more pressure drop in channel. But the THPEC index analyze the both above parameters with each other and when the THPEC is more than 1, usage of nanofluid is in view point of thermal and hydraulic performance appropriate and efficient. For the nanofluid with diameter size of 50 nm and volume fraction of 4% the maximum values of THPEC are achieved for all investigated Re, which is followed with cases $d_{np} = 40$ nm, 30 nm and 20 nm, respectively⁴⁸.

Finally, usage of H_2O 99.5%:0.5% CMC/ Al_2O_3 nanofluid in nanoparticle volume concentration of $\phi = 4\%$ and nanoparticle diameter of $d_{np} = 50$ nm through helical heat exchanger equipped with corrugated channel with novel turbulators is suggested in paper as the optimum mode; with the maximum THPEC index at Re = 5000.

Also Fig. 17 illustrates economic, the THPEC index variation at Re = 5000 in helical heat exchanger with novel turbulators saturated with nanofluid ($\phi = 4\%$ and $d_{np} = 50$ nm) in comparison with basic system. This figure shows that using novel heat exchanger instead of the basic smooth system, the thermal properties (by considering Nusselt number) increases about 210%, the hydraulic performance (friction factor) reduces about 28%, performance evaluation criteria index increases about 57% and the material consumption (in case of similar thermal-hydraulic performance) decreases about 31%. In another word, for the basic and novel system which has same efficiencies, the novel one has lower length and consequently 31% lower material.

Conclusion

Thermal-hydraulic analysis of a helical heat exchanger with novel turbulators saturated with two-phase NNNF has been done. The major obtained results are:

- Using corrugated channel in helical heat exchanger has a considerable influence on the THPEC index of heat exchanger and can improve the THPEC index in heat exchanger.
- $Re = 5000$ is an optimum Reynolds number, in which the maximum THPEC value is achieved.
- It is clear that in case of using turbulators two parameters have increase: heat transfer rate (Nu_{avg}) and pressure reduction penalty.
- In case of employing nanofluid two parameters have increase: Nu_{av} and pressure reduction penalty.
- For the nanofluid with constant volume fraction, the maximum values of THPEC are achieved for all investigated Re for nanoparticles diameter of 50 nm, which is followed with cases $\phi = 3\%$, 2% and 1%, respectively.
- For the nanofluid with constant diameter size, the maximum values of THPEC are achieved during all investigated Re for volume fraction of 4%, which is followed with cases $d_{np} = 40$ nm, 30 nm and 20 nm, respectively.
- Usage of H_2O 99.5%:0.5% CMC/ Al_2O_3 nanofluid in nanoparticle volume concentration of $\phi = 4\%$ and nanoparticle diameter of $d_{np} = 50$ nm through helical heat exchanger equipped with corrugated channel with novel turbulators is suggested in paper as the optimum mode; with the maximum THPEC index at $Re = 5000$.
- For the basic and novel system which has same efficiencies, the novel one has lower length and consequently 31% lower material.

Received: 25 December 2020; Accepted: 17 May 2021

Published online: 02 June 2021

References

1. Arie, M. A., Hymas, D. M., Singer, F., Shooshtari, A. H. & Ohadi, M. An additively manufactured novel polymer composite heat exchanger for dry cooling applications. *Int. J. Heat Mass Transf.* **147**, 118889 (2020).
2. Bezaatpour, M. & Rostamzadeh, H. Heat transfer enhancement of a fin-and-tube compact heat exchanger by employing magnetite ferrofluid flow and an external magnetic field. *Appl. Therm. Eng.* **164**, 114462 (2020).
3. Abeykoon, C. Compact heat exchangers – Design and optimization with CFD. *Int. J. Heat Mass Transf.* **146**, 118766 (2020).
4. Saleh, M. M., Al-Dadah, R., Mahmoud, S., Elsayed, E. & El-Samni, O. Wire fin heat exchanger using aluminium fumarate for adsorption heat pumps. *Appl. Therm. Eng.* **164**, 114426 (2020).
5. Hagen, B. A. L., Nikolaisen, M. & Andresen, T. A novel methodology for Rankine cycle analysis with generic heat exchanger models. *Appl. Therm. Eng.* **165**, 114566 (2020).
6. Larwa, B. & Kupiec, K. Heat transfer in the ground with a horizontal heat exchanger installed – Long-term thermal effects. *Appl. Therm. Eng.* **164**, 114539 (2020).
7. Naicker, S. S. & Rees, S. J. Long-term high frequency monitoring of a large borehole heat exchanger array. *Renewable Energy* **145**, 1528–1542 (2020).
8. Warner, J., Liu, X., Shi, L., Qu, M. & Zhang, M. A novel shallow bore ground heat exchanger for ground source heat pump applications—Model development and validation. *Appl. Therm. Eng.* **164**, 114460 (2020).
9. Hu, Y., Heiselberg, P. K., Johra, H. & Guo, R. Experimental and numerical study of a PCM solar air heat exchanger and its ventilation preheating effectiveness. *Renewable Energy* **145**, 106–115 (2020).
10. Kumar Agrawal, K., Misra, R. & Das Agrawal, G. Improving the thermal performance of ground air heat exchanger system using sand-bentonite (in dry and wet condition) as backfilling material. *Renewable Energy* **146**, 2008–2023 (2020).
11. Wen, Z.-X., Lv, Y.-G., Li, Q. & Zhou, P. Numerical study on heat transfer behavior of wavy channel supercritical CO_2 printed circuit heat exchangers with different amplitude and wavelength parameters. *Int. J. Heat Mass Transf.* **147**, 118922 (2020).
12. Chu, W.-X., Sheu, W.-J., Hsu, C.-C. & Wang, C.-C. Airside performance of sinusoidal wavy fin-and-tube heat exchangers subject to large-diameter tubes with round or oval configuration. *Appl. Therm. Eng.* **164**, 114469 (2020).
13. Yu, C., Zhang, H., Zeng, M., Wang, R. & Gao, B. Numerical study on turbulent heat transfer performance of a new compound parallel flow shell and tube heat exchanger with longitudinal vortex generator. *Appl. Therm. Eng.* **164**, 114449 (2020).
14. Habibi, M., Amadeh, A. & Hakkaki-Fard, A. A numerical study on utilizing horizontal flat-panel ground heat exchangers in ground-coupled heat pumps. *Renewable Energy* **147**(1), 996–1010 (2020).
15. Kerme, E. D. & Fung, A. S. Heat transfer simulation, analysis and performance study of single U-tube borehole heat exchanger. *Renewable Energy* **145**, 1430–1448 (2020).
16. Mohammed, H. A., Gunnasegaran, P. & Shuaib, N. H. Numerical simulation of heat transfer enhancement in wavy microchannel heat sink. *Int. Commun. Heat Mass Transf.* **38**(1), 63–68 (2011).
17. Shahzad Nazir, M. *et al.* A comprehensive review of parabolic trough solar collectors equipped with turbulators and numerical evaluation of hydrothermal performance of a novel model. *Sustain. Energy Technol. Assess.* **45**, 101103 (2021).
18. Manca, O., Nardini, S. & Ricci, D. A numerical study of nanofluid forced convection in ribbed channels. *Appl. Therm. Eng.* **37**, 280–292 (2012).
19. Rostami, S. *et al.* A review of melting and freezing processes of PCM/nano-PCM and their application in energy storage. *Energy* **211**, 118698 (2020).
20. Niknejadi, M., Afrand, M., Karimipour, A., Shahsavari, A. & MeghdadiIsfahani, A. H. Experimental investigation of the hydrothermal aspects of water- Fe_3O_4 nanofluid inside a twisted tube. *J. Therm. Anal. Calorimetry* **143**, 801–810 (2021).
21. Ahmed, M. A., Shuaib, N. H., Yusoff, M. Z. & Al-Falahi, A. H. Numerical investigations of flow and heat transfer enhancement in a corrugated channel using nanofluid. *Int. Commun. Heat Mass Transf.* **38**(10), 1368–1375 (2011).
22. Li, Z. X. *et al.* Multi-objective energy and exergy optimization of different configurations of hybrid earth-air heat exchanger and building integrated photovoltaic/thermal system. *Energy Convers. Manag.* **195**, 1098–1110 (2019).
23. Niknejadi, M., Afrand, M., Karimipour, A., Shahsavari, A. & Isfahani, A. H. M. An experimental study on the cooling efficiency of magnetite–water nanofluid in a twisted tube exposed to a rotating magnetic field. *J. Therm. Anal. Calorim.* **1**, 1–17 (2020).
24. AbbasianArani, A. A., Sadripour, S. & Kermani, S. Nanoparticle shape effects on thermal-hydraulic performance of boehmite alumina nanofluids in a sinusoidal–wavy mini-channel with phase shift and variable wavelength. *Int. J. Mech. Sci.* **128–129**, 550–563 (2017).
25. Sadripour, S., Ghorashi, S. A. & Estajloo, M. Numerical investigation of a cavity equipped with corrugated heat source: A full convection-conduction-radiation coupling. *Am. J. Aerosp. Eng.* **4**(3), 27–37 (2017).
26. Heris, S. Z., Esfahany, M. N. & Etemad, G. Numerical investigation of nanofluid laminar convective heat transfer through a circular tube. *Numer. Heat Transf. Part A Appl.* **52**(11), 1043–1058 (2017).
27. Heris, S. Z., Etemad, S. G. & Esfahany, M. N. Convective heat transfer of a Cu/water nanofluid flowing through a circular tube. *Exp. Heat Transf.* **22**(4), 217–227 (2019).

28. Keshavarz Moraveji, M., Haddad, S. M. H. & Darabi, M. Modeling of forced convective heat transfer of a non-Newtonian nanofluid in the horizontal tube under constant heat flux with computational fluid dynamics. *Int. Commun. Heat Mass Transf.* **39**, 995–999 (2012).
29. Akbari, O. A., Toghraie, D., Karimipour, A., Marzban, A. & Ahmadi, G. R. The effect of velocity and dimension of solid nanoparticles on heat transfer in non-Newtonian nanofluid. *Phys. E*. **86**, 68–75 (2017).
30. Minea, A. A. Uncertainties in modeling thermal conductivity of laminar forced convection heat transfer with water alumina nanofluids. *Heat Mass Transf.* **68**, 78–84 (2014).
31. Zeinali Heris, S., Etemad, S.Gh. & Nasr Esfahany, M. Numerical investigation of nanofluid laminar convective heat transfer through a circular tube. *Numer. Heat Transf. Part A: Appl.* **52**(11), 1043–1058 (2007).
32. Gholami, M. R. *et al.* The effect of rib shape on the behavior of laminar flow of oil/MWCNT nanofluid in a rectangular microchannel. *J. Therm. Anal. Calorim.* **134**, 1611–1628. <https://doi.org/10.1007/s10973-017-6902-3> (2018).
33. Zadeh, A. D. & Toghraie, D. Experimental investigation for developing a new model for the dynamic viscosity of silver/ethylene glycol nanofluid at different temperatures and solid volume fractions. *J. Therm Anal Calorim* **131**, 1449–1461. <https://doi.org/10.1007/s10973-017-6696-3> (2018).
34. Khodadadi, H., Toghraie, D. & Karimipour, A. Effects of nanoparticles to present a statistical model for the viscosity of MgO-Water nanofluid. *Powder Technol.* **342**, 166–180 (2019).
35. Goodarzi, M. *et al.* Experimental evaluation of dynamic viscosity of ZnO–MWCNTs/engine oil hybrid nanolubricant based on changes in temperature and concentration. *J. Therm. Anal. Calorim.* **136**, 513–525. <https://doi.org/10.1007/s10973-018-7707-8> (2019).
36. Sarlak, R. *et al.* The investigation of simultaneous heat transfer of water/Al₂O₃ nanofluid in a close enclosure by applying homogeneous magnetic field. *Int. J. Mech. Sci.* **133**, 674–688 (2017).
37. Arasteh, H. *et al.* Optimal arrangements of a heat sink partially filled with multilayered porous media employing hybrid nanofluid. *J. Therm. Anal. Calorim.* **137**, 1045–1058. <https://doi.org/10.1007/s10973-019-08007-z> (2019).
38. Saeedi, A. H., Akbari, M. & Toghraie, D. An experimental study on rheological behavior of a nanofluid containing oxide nanoparticle and proposing a new correlation. *Phys. E: Low-dimens. Syst. Nanostruct.* **99**, 285–293 (2018).
39. Mohammed, H. A., Abuobeidab, I. A. M. A., Vuthaluru, H. B. & Liua, S. Two-phase forced convection of nanofluids flow in circular tubes using convergent and divergent conical rings inserts. *Int. Commun. Heat Mass Transfer* **101**, 10–20 (2019).
40. Karimi, A. *et al.* The effects of tape insert material on the flow and heat transfer in a nanofluid-based double tube heat exchanger: Two-phase mixture model. *Int. J. Mech. Sci.* **156**, 397–409 (2019).
41. Sheikholeslami, M. & Rokni, H. B. Influence of melting surface on MHD nanofluid flow by means of two phase model. *Chin. J. Phys.* **55**(4), 1352–1360 (2018).
42. Sheikholeslami, M. & Rokni, H. B. Nanofluid two phase model analysis in existence of induced magnetic field. *Int. J. Heat Mass Transf.* **107**, 288–299 (2017).
43. Alsarraf, J. *et al.* Hydrothermal analysis of turbulent boehmite alumina nanofluid flow with different nanoparticle shapes in a minichannel heat exchanger using two-phase mixture model. *Phys. A* **520**, 275–288 (2019).
44. Ansys® Academic Research Mechanical, Release 18, Help System, Coupled Field Analysis Guide, ANSYS, Inc.
45. Barnoon, P., Toghraie, D., Eslami, F. & Mehmandoust, B. Entropy generation analysis of different nanofluid flows in the space between two concentric horizontal pipes in the presence of magnetic field: Single-phase and two-phase approaches. *Comput. Math. Appl.* **77**(3), 662–692 (2019).
46. Arani, A. A. & Moradi, R. Shell and tube heat exchanger optimization using new baffle and tube configuration. *Appl. Thermal Eng.* **157**, 113736 (2019).
47. Li, B., Zhang, W., Zhu, L., Lin, Y. & Bai, B. Effects of nanoparticle migration on non-Newtonian nanofluids in a channel with multiple heating and cooling regions. *Int. J. Heat Mass Transf.* **107**, 836–845 (2017).
48. Santra, A. K., Sen, S. & Chakraborty, N. Study of heat transfer due to laminar flow of copper–water nanofluid through two isothermally heated parallel plates. *Int. J. Thermal Sci.* **48**, 391–400 (2009).
49. Kamali, R. & Binesh, A. R. Numerical investigation of heat transfer enhancement using carbon nanotube non-Newtonian nanofluids. *Int. Commun. Heat Mass Transfer* **37**, 1153–1157 (2010).
50. Asadi, A. & Pourfath, F. Heat transfer performance of two oil-based nanofluids containing ZnO and MgO nanoparticles; a comparative experimental investigation. *Powder Technol.* **343**, 296–308 (2019).
51. S.V., Patankar, "Numerical Heat Transfer and Fluid Flow", Taylor & Francis Group, 1980.
52. Garoosi, F. Presenting two new empirical models for calculating the effective dynamic viscosity and thermal conductivity of nanofluids. *Powder Technol.* **366**, 788–820 (2020).
53. Garoosi, F. & MehdiRashidi, M. Two phase flow simulation of conjugate natural convection of the nanofluid in a partitioned heat exchanger containing several conducting obstacles. *Int. J. Mech. Sci.* **130**, 282–306 (2017).
54. Garoosi, F. & Talebi, F. Numerical analysis of conjugate natural and mixed convection heat transfer of nanofluids in a square cavity using the two-phase method. *Adv. Powder Technol.* **28**(7), 1668–1695 (2017).
55. Garoosi, F. & Talebi, F. Numerical simulation of conjugate conduction and natural convection heat transfer of nanofluid inside a square enclosure containing a conductive partition and several disconnected conducting solid blocks using the Buongiorno's two phase model. *Powder Technol.* **317**, 48–71 (2017).
56. Garoosi, F. & Mehdi Rashidi, M. Conjugate-mixed convection heat transfer in a two-sided lid-driven cavity filled with nanofluid using Manninen's two phase model. *Int. J. Mech. Sci.* **131–132**, 1026–1048 (2017).
57. Launder, B. E. & Spalding, D. B. The numerical computation of turbulent flows. *Comput. Methods Appl. Mech. Eng.* **3**, 269–289. [https://doi.org/10.1016/0045-7825\(74\)90029-2](https://doi.org/10.1016/0045-7825(74)90029-2) (1974).
58. Van Driest, E. R. On turbulent flow near a wall. *J. Aeronaut. Sci.* **23**(11), 1007–1011. <https://doi.org/10.2514/8.3713> (1956).
59. Corcione, M. Empirical correlating equations for predicting the effective thermal conductivity and dynamic viscosity of nanofluids. *Energy Convers. Manag.* **52**, 789–793 (2011).
60. Gupta, S. & Varshney, P. K. Effect of plasticizer on the conductivity of carboxymethyl cellulose-based solid polymer electrolyte. *Polym. Bull.* **76**, 6169–6178. <https://doi.org/10.1007/s00289-019-02714-1> (2019).
61. Kim, D. *et al.* Convective heat transfer characteristics of nanofluids under laminar and turbulent flow conditions. *Curr. Appl. Phys.* **9**(2), 119–123 (2009).

Acknowledgements

The authors gratefully acknowledge financial support from the German Research Foundation (DFG).

Author contributions

M.I., E.A., T.S., A.B., Y.C., and G.C. wrote the manuscript. M.I., E.A., T.S., A.B., Y.C., and G.C. provided critical feedback and helped shape the research, analysis, and manuscript. All authors discussed the results and commented on the manuscript.

Funding

Open Access funding enabled and organized by Projekt DEAL.

Competing interests

The authors declare no competing interests.

Additional information

Correspondence and requests for materials should be addressed to Y.-M.C. or G.C.

Reprints and permissions information is available at www.nature.com/reprints.

Publisher's note Springer Nature remains neutral with regard to jurisdictional claims in published maps and institutional affiliations.



Open Access This article is licensed under a Creative Commons Attribution 4.0 International License, which permits use, sharing, adaptation, distribution and reproduction in any medium or format, as long as you give appropriate credit to the original author(s) and the source, provide a link to the Creative Commons licence, and indicate if changes were made. The images or other third party material in this article are included in the article's Creative Commons licence, unless indicated otherwise in a credit line to the material. If material is not included in the article's Creative Commons licence and your intended use is not permitted by statutory regulation or exceeds the permitted use, you will need to obtain permission directly from the copyright holder. To view a copy of this licence, visit <http://creativecommons.org/licenses/by/4.0/>.

© The Author(s) 2021